Nanoscale Horizons

The home for rapid reports of exceptional significance in nanoscience and nanotechnology

rsc.li/nanoscale-horizons

ROYAL SOCIETY
OF CHEMISTRY
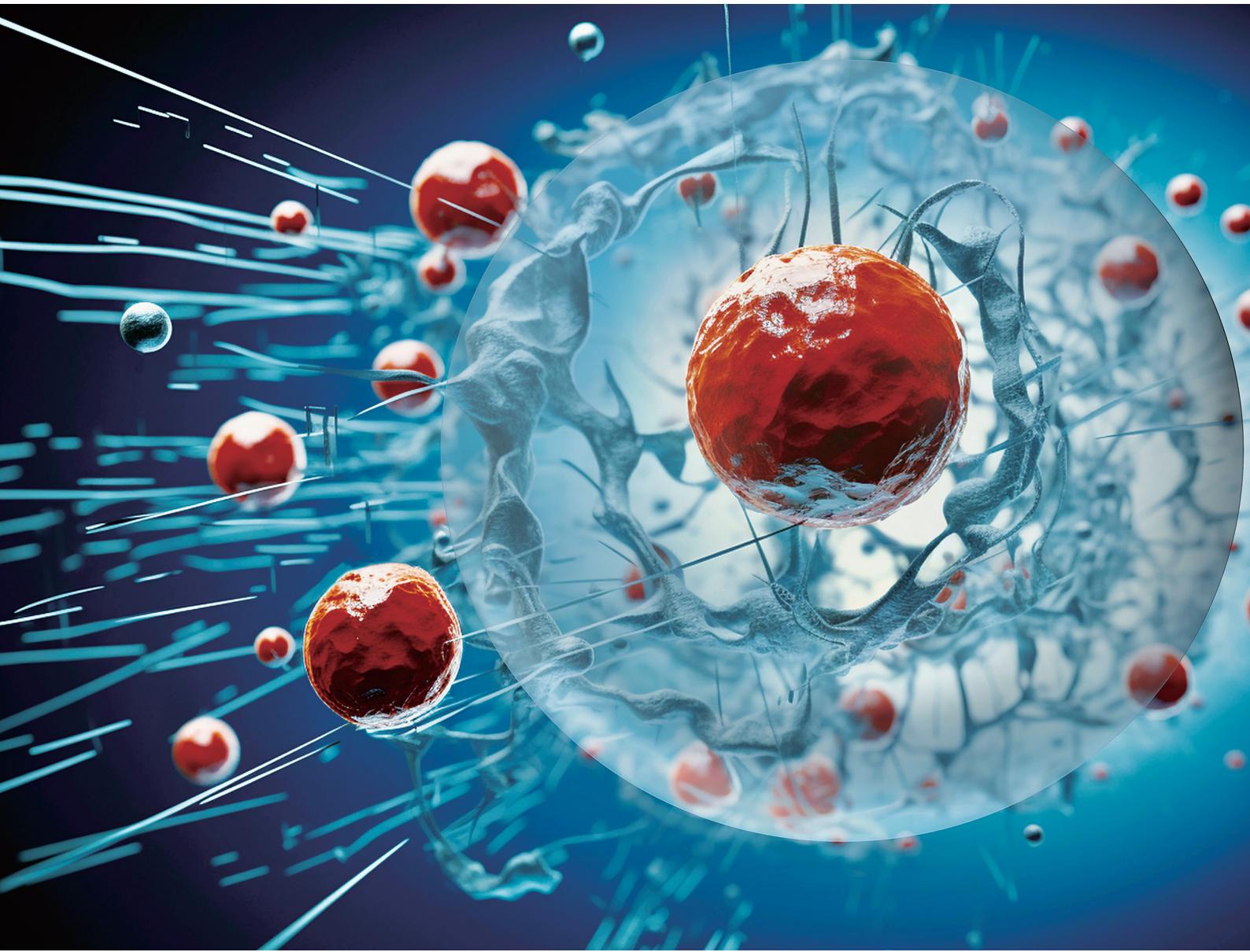
COMMUNICATION
Hang Jiang, To Ngai *et al.*
Pickering emulsion templated proteinaceous microparticles
as glutathione-responsive carriers for endocytosis in tumor
cells

NCNST

COMMUNICATION

Check for updates

Pickering emulsion templated proteinaceous microparticles as glutathione-responsive carriers for endocytosis in tumor cells†

Weijie Jiang,‡[a] Xin Guan, [iD]‡[b] Wei Liu, [iD][a] Yunxing Li, [iD][a] Hang Jiang [iD]*[a] and To Ngai [iD]*[b]

The use of glucose oxidase (GOx) to disrupt glucose supply has been identified as a promising strategy in cancer starvation therapy. However, independent delivery of GOx is prone to degradation upon exposure to biological conditions and may cause damage to blood vessels and normal organs during transportation. Although some carriers can protect GOx from the surrounding environment, the harsh preparation conditions may compromise its activity. Moreover, the commonly used materials often exhibit poor biocompatibility and possess certain cytotoxicity. To address this issue, we developed a gentle and efficient method based on Pickering emulsion templates to synthesize protein-based microparticles using zein as the matrix material. These microparticles have high stability and can be tailored to efficiently encapsulate biomolecules while preserving their activity. Moreover, the zein-based microparticles can be triggered to release biomolecules in tumor cells under high glutathione levels, demonstrating excellent responsiveness, biocompatibility, and low cytotoxicity. Additionally, when loaded with GOx, these protein-based microparticles effectively deprive tumor cells of nutrients and induce apoptosis by generating high levels of H_2O_2, thereby exhibiting enhanced anticancer properties.

New concepts

Zein, a corn-derived protein, is widely recognized for its biocompatibility, biodegradability, and cost-effectiveness, rendering it highly suitable for various delivery systems. However, conventional anti-solvent techniques employed in zein particle synthesis often encounter challenges such as aggregation, substance leakage, and low drug loading. Surfactants or crosslinkers, commonly employed to address these issues, may compromise the biosafety of the resulting particles. To overcome these limitations, we propose an eco-friendly Pickering emulsion method for the fabrication of zein microparticles. This innovative technique offers stable and tunable structures while achieving high encapsulation efficiency of biomolecules, thereby preserving their biological activity. Notably, these zein microparticles exhibit a distinctive responsiveness to glutathione (GSH), a crucial molecule found in abundance in tumor cells. This unique property allows the microparticles to disintegrate specifically in GSH-rich tumor cells without the need for chemical grafting. To validate this concept, we encapsulated glucose oxidase (GOx) within the zein microparticles for potential application in starvation therapy. This approach provides a simpler and more environmentally friendly alternative to conventional methods, eliminating the need for harsh conditions or toxic chemicals. The development of such zein-based microparticles opens up new avenues for biomedical applications, paving the way for advancements in targeted drug delivery and therapeutic interventions.

1. Introduction

Cancer remains a leading cause of mortality, creating a significant health challenge worldwide.[1] In the pursuit of effective cancer treatments,[2–7] researchers have become increasingly interested in understanding the role of glucose as a primary energy source for tumor cells. Glucose oxidase (GOx), an enzyme that decomposes glucose in the presence of oxygen (O_2), has shown potential in starving tumor cells of their energy supply. Furthermore, the breakdown of glucose by GOx leads to the production of hydrogen peroxide (H_2O_2), a highly toxic compound that can prove lethal to tumor cells.[8–12] This innovative approach, known as GOx-based "starvation therapy", has garnered significant attention in the field of biomedical research.[13,14]

Despite its promising antitumor potential, the therapeutic use of GOx is limited due to its vulnerability to biological degradation, particularly in the demanding physiological environments of the human body.[15,16] To overcome this challenge, recent advances in anticancer therapy have focused on the targeted delivery of micro/nano carriers to tumors.[17–20] However, most of the available carriers

[a] Key Laboratory of Synthetic and Biological Colloids, Ministry of Education & School of Chemical and Material Engineering, Jiangnan University, Wuxi, P. R. China. E-mail: hangjiang@jiangnan.edu.cn

[b] Department of Chemistry, The Chinese University of Hong Kong, Shatin, N. T., Hong Kong. E-mail: tongai@cuhk.edu.hk

† Electronic supplementary information (ESI) available. See DOI: https://doi.org/10.1039/d3nh00551h

‡ These authors contribute equally to the work.

are synthetic polymers, which may trigger immune reactions or chronic inflammation, thereby restricting their biomedical applications.[21]

In contrast, proteinaceous carriers provide substantial advantages compared to synthetic polymers, and employing proteins as precursor materials frequently leads to low immunogenicity.[22–24] Zein, with its unique composition and structure, exhibits excellent properties for film formation, biocompatibility, biodegradability, acid resistance, and self-assembly.[25–27] These characteristics make zein an ideal candidate for controlled release and targeted delivery in biomedicine.[28,29] In addition, zein contains peptides of varying sizes, solubilities, and charges, connected by disulfide bonds. These bonds can be reinforced through solvent evaporation during zein concentration,[30] enabling the creation of reduction-responsive carriers without the need for additional modification. The intracellular level of glutathione (GSH) is significantly increased in cancer cells compared to normal tissue cells, creating an environment with high reductive capacity.[31–33] Therefore, the reduction-responsive carriers can effectively enhance anti-cancer activity.[34–36] Various methods exist for preparing zein-based particles, including antisolvent,[37] chemical crosslinking,[38] and emulsification techniques.[39] Among these approaches, the emulsification method stands out due to its simplicity and the ability to control particle morphology. Emulsification techniques have also been found to enhance the encapsulation of active substances, making them a preferred choice for particle fabrication. However, the use of traditional surfactants for emulsion stabilization requires immediate processing to prevent demulsification, which can hinder particle formation.[40]

To address these challenges, we have developed zein-based microparticles using a one-pot Pickering emulsion method, building upon our previous research.[41,42] This innovative approach overcomes issues related to biocompatibility losses by keeping the internal and external phases of the emulsion separate.[43–45] In this way, it minimizes the leakage of therapeutic biomolecules and enhances encapsulation efficiency. Furthermore, these zein-based microparticles possess a unique characteristic of disintegration at high GSH levels. This GSH-dependent dissociation allows for the responsive release of encapsulated biomolecules. Next, GOx was selected for encapsulation within the zein-based microparticles. The aim is to protect GOx and enhance its targeted delivery to tumor cells, thereby facilitating effective therapeutic action.

2. Results and discussion

The design and synthesis process of GSH-responsive zein-based microparticles is illustrated in Scheme 1. Initially, a Pickering double emulsion template was prepared by sonicating the mixture of ethanol/water phase containing zein, GOx, and oil phase containing hydrophobic CaCO$_3$ nanoparticles. After removing ethanol and oil phases, GOx was successfully encapsulated inside the microparticles with a colloidal CaCO$_3$ shell. This is because zein precipitated on the surface of the droplet during phase evaporation, in which CaCO$_3$ nanoparticles
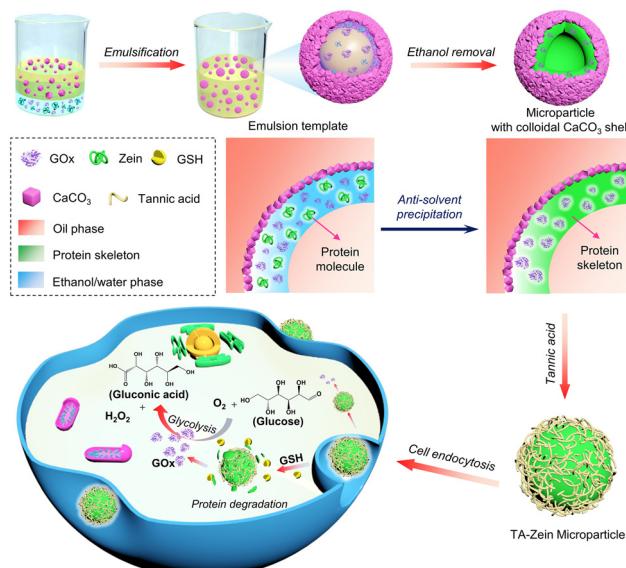
Scheme 1 Schematic illustration of the fabrication of GSH-responsive zein-based microparticles for starvation therapy.

attached to the zein skeleton due to the composition changes of the ethanol/water phase. The CaCO$_3$ nanoparticles on the microparticle surfaces could be removed using tannic acid (TA), the resulting TA/zein microparticles were then transferred to the aqueous phase and could enter into tumor cells through endocytosis. Within the intracellular environment, the microparticles would deconstruct, as the disulfide bonds between zein molecules were cleaved due to the high concentration of GSH in tumor cells. This process ultimately led to the release of GOx, which induces starvation therapy for tumor cells.

Characterization of CaCO$_3$/zein microparticles

Firstly, an aqueous solution of zein was mixed at an (ethanol/water)/oil volume fraction of 0.05 and sonicated to create a Pickering double emulsion template stabilized by CaCO$_3$ nanoparticles (Fig. S1a, ESI†). In this process, the hydrophobic CaCO$_3$ nanoparticles serve as a solid emulsifier because zein alone is unable to stabilize the emulsion (Fig. S1b, ESI†). By removing ethanol and oil, a hybrid microparticle was effectively produced. Scanning electron microscope (SEM) (Fig. 1a and b) and transmission electron microscope (TEM) images (Fig. S2, ESI†) show that the resulting CaCO$_3$/zein microparticles collapsed after the drying process, while their structure remained intact. A magnified image of the microparticle surface reveals that the CaCO$_3$ nanoparticles are densely packed to form a protective layer (Fig. 1c). As shown in Fig. 1d and e, the resultant microparticles with an average size of 1.2 μm (Fig. 1f) were able to disperse well in dodecane due to the hydrophobic nature of the adsorbed CaCO$_3$ nanoparticles on the surface. To visualize the structure of the CaCO$_3$/zein microparticles more directly, rhodamine B (red channel) and perylene (blue channel) were employed to stain zein protein and dodecane, respectively (Fig. S3, ESI†). We further synthesized larger microparticles with a size of approximately 50 μm to better distinguish the interior
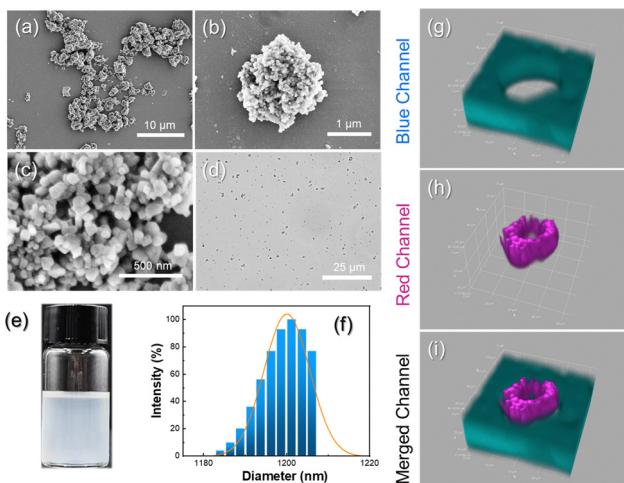
Fig. 1 SEM images (a)–(c) and corresponding size distribution (f) of the CaCO$_3$/zein microparticles. Optical microscope image (d) and photograph (e) of the microparticles dispersed in the oil phase. 3D confocal images (g)–(i) of the microparticles, in which zein and oil phases were separately labelled with rhodamine B (red) and perylene (blue).

Fig. 2 Photographs and SEM images of CaCO$_3$/zein microparticles dispersed in an aqueous solution (a) and treated with 0.001 M HCl (b).

structure. As shown in confocal laser scanning microscopy (CLSM) (Fig. 1g–i), a hollow cavity is clearly visible inside the microparticles. The red circle represents a thick shell of precipitated zein protein, resulting from the formation of an oil-in-(ethanol/water)-in-oil Pickering double emulsion.

To acquire a suitable size for cellular endocytosis, the average diameter of the CaCO$_3$/zein microparticles was precisely controlled by adjusting the emulsification parameters. It was observed that increasing the concentration of CaCO$_3$ nanoparticles from 0.5 wt% to 5 wt% resulted in a reduction in the mean size of the microparticles (Fig. S4, ESI†). Likewise, the method of emulsification and water–oil ratio was also optimized, and it was concluded that higher sonication power and larger water–oil ratio led to the generation of smaller microparticles (Fig. S5 and S6, ESI†). Based on these experimental results, 5 wt% CaCO$_3$ nanoparticles, 600 W sonication, and 0.05 water–oil ratio were selected for the ideal preparation of microparticles.

Construction of TA/zein microparticles

Considering the living environment of cells, it is necessary for the enzyme-carrying microparticles to be well dispersed in the aqueous medium. However, Fig. 2a shows that a significant amount of powder floated on the surface of the aqueous solution. Consequently, the efficacy of the microparticles in the subsequent cell assays is compromised. To address this issue, we suspected that the dispersibility of microparticles could be improved by utilizing acid to decompose CaCO$_3$. By subjecting microparticles to 0.001 M HCl, the CaCO$_3$ nanoparticles on the microparticle surfaces were removed by a subsequent washing process. It is worth noting that the isoelectric point of zein protein is approximately 6.5. To avoid inducing aggregation to zein proteins, the pH of the microparticle dispersion was controlled between 3 and 5 to ensure
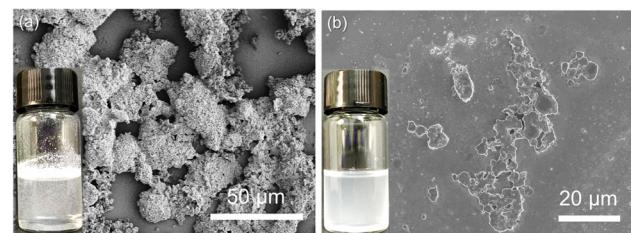
their stability in water.[46] Fig. 2b indicates that the dispersity of HCl-treated microparticles underwent a significant improvement while numerous agglomerates still existed in the dispersion. The HCl-treated CaCO$_3$/zein microparticles were then used to co-culture with HeLa cells for 24 h. It is evident that they continue to form large aggregates in the medium, with minimal instances of endocytic particles observed in the overlay figure (Fig. S7, ESI†). Consequently, it is ineffective for subsequent cell studies.

Tannic acid (TA), a polyphenol found abundantly in plants, offers dual functionalities in the removal of CaCO$_3$ nanoparticles due to its acidity and numerous phenolic hydroxyl groups can interact with proteins by hydrogen bonding and hydrophobic interactions.[47,48] Fig. 3a illustrates the process of treating CaCO$_3$/zein microparticles with TA. As shown in Fig. S8 (ESI†), when the ratio of TA to the hybrid microparticles reached 10 : 1, no visible powder appeared in the upper layer of the suspension, suggesting that their hydrophilicity was highly improved. As displayed in Fig. 3b, CaCO$_3$ nanoparticles exhibited high hydrophobicity with the water contact angle approaching 140°. Similarly, the CaCO$_3$/zein microparticles also exhibited a large water contact angle of over 120°, thus making it difficult for them to be dispersed effectively in water. In contrast, the TA treatment led to a significant reduction in the water contact angle of the CaCO$_3$/zein microparticles (about 20°), consistent with the above phenomenon. The size distribution of TA/zein microparticles is shown in Fig. S9 (ESI†), with an average particle size slightly smaller than the aforementioned CaCO$_3$/zein
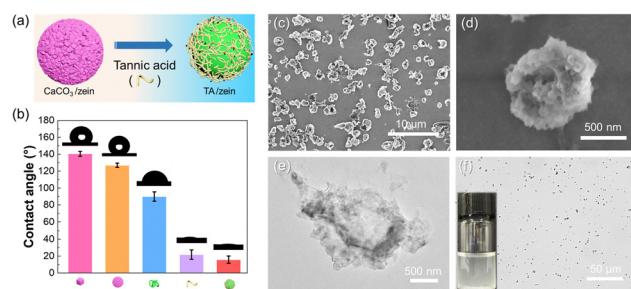

Fig. 3 (a) Schematic representation of the procedure for tannic acid (TA) treatment. (b) The water contact angle of the hydrophobic CaCO$_3$ nanoparticles, the CaCO$_3$/zein microparticles, zein powder, tannic acid powder, and TA/zein microparticles. SEM images (c), (d) and TEM image (e) of the TA/zein microparticles. (f) Picture and optical microscopy image of the water-dispersed TA/zein microparticles.

microparticles. This is primarily due to the decomposition of the surface $CaCO_3$ nanoparticles. After drying, the morphology of the resulting TA/zein microparticles was visualized using SEM and TEM, as shown in Fig. 3c–e. Although the surface of the microparticle structure exhibited wrinkling, it still maintained intact without significant fracture. Besides, it is apparent that the microparticle surface is smooth and devoid of excess $CaCO_3$ particles. This observation suggests that a specific concentration of TA is capable of decomposing $CaCO_3$ nanoparticles. Furthermore, excessive TA can bind to zein, ensuring the good dispersion of the TA/zein microparticles in the medium and preventing agglomeration (Fig. 2f).

We then used Fourier transform infrared spectroscopy (FTIR) to elucidate the interaction between different components of the microparticles and analyse their chemical structure (Fig. S10, ESI†). The broad adsorption peak between 3200–3400 cm^{-1} can be attributed to the hydroxyl stretching vibration. The amide I and amide II bands of zein are located at 1645 cm^{-1} ($\nu(C{=}O)$) and 1532 cm^{-1} ($\nu(C{-}N)$), respectively. On the other hand, TA displays three absorption peaks at 1699 cm^{-1}, 1606 cm^{-1}, and 1532 cm^{-1}, which correspond to the characteristic peaks of ester bonds in TA molecules. Comparing the IR spectrum of zein and TA-zein, the amide I band and amide II of the pure protein are shifted to 1652 cm^{-1} and 1532 cm^{-1}, respectively. These findings suggest that electrostatic interactions also contribute to the co-assembly of the TA/zein microparticles.

GSH-Triggered release of FITC-dextran *in Vitro*

Due to the presence of GSH within cancer cells, the disulfide bond between zein protein molecules could be disrupted, resulting in the rupture of the microparticles and release of loaded active cargos. Therefore, FITC-dextran (70 kDa) was chosen as a fluorescent model active. Firstly, we conducted an evaluation of the encapsulation efficiency of TA-zein nanoparticles. The encapsulation rate of FITC-dextran by TA-zein microparticles was determined to be approximately 82.8%, as indicated by the fluorescence intensity curve depicted in Fig. S11 (ESI†). Comparatively, the encapsulation rate achieved through the traditional anti-solvent method was found to be only 53.1%. The Pickering emulsion method, on the other hand, significantly improves the encapsulation efficiency and minimizes the loss of active substances. We subsequently investigated the release behavior of the microparticles induced by GSH at different times, as depicted in Fig. 4a.

To evaluate the release profile of active cargos in the microparticles, the morphologies of the microparticles were observed by CLSM. It was observed that the inclusion of FITC-dextran remained confined and showed green fluorescence within the microparticle shell even after exposure to TA (Fig. S12, ESI†). Subsequently, GSH solutions of different concentrations (0 mM, 5 mM, and 10 mM) were prepared and added sequentially to the aqueous solution containing TA/zein microparticles loaded with FITC-dextran. The fluorescence intensity of the solution was measured at various time points along with different concentrations of GSH (Fig. S13, ESI†). The release profile of FITC-dextran was further determined for each of the
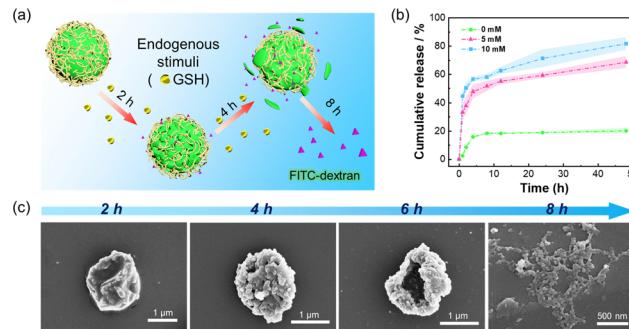

Fig. 4 (a) Schematic representation of active cargo release induced by GSH stimuli over time. (b) Release curves of the TA/zein microparticles at different concentrations of GSH. (c) A time series of the SEM images shows the dissolution of protein skeleton at 10 mM GSH.

three GSH concentrations, and Fig. 4b demonstrates a clear correlation between the GSH concentration and the release of FITC-dextran. Specifically, the release profile experienced a significant increase in the first several hours and then only slightly increased. In addition, the release of FITC-dextran was highly dependent on the GSH concentration. A higher GSH concentration (10 mM) can induce 20% and 60% more release ratio of FITC-dextran than 5 mM and 0 mM GSH. These results indicate that the release behavior of the microparticles can be manipulated by adjusting the GSH concentrations. We then used SEM to verify the effect of GSH on the structural integrity of the TA/zein microparticles. Before the morphology observation, the TA/zein microparticle suspensions were exposed to 10 mM GSH for 2 h, 4 h, 6 h, and 8 h, respectively. As shown in Fig. 4c, the microparticle structure gradually collapsed and ruptured over time. The complete disintegration of the microparticles occurred at 8 h, demonstrating that the release of the loaded cargos was attributed to the GSH-induced decomposition of the proteinaceous shell.

Catalytic performance of GOx@TA/zein microparticles

The rapid metabolism of tumor sites leads to a unique tumor microenvironment. The well-developed blood vessels within the tumor promote the rapid growth of tumor cells by supplying them with essential nutrition, particularly glucose. According to the Warburg effect,[49,50] tumor cell proliferation mainly relies on aerobic glycolysis, making them highly susceptible to changes in glucose levels. Consequently, altering the glucose metabolism pathway inside tumor cells is an effective and safe strategy for cancer treatment. GOx can consume glucose within tumor sites, thereby disrupting the nutrient supply and generating a high concentration of H_2O_2, which shows a synergistic effect in killing cancer cells. Therefore, GOx was chosen as a therapeutic biomolecule and subsequently encapsulated into TA/zein microparticles.

After loading GOx inside the microparticles, we assessed the catalytic performance of GOx@TA/zein microparticles. Amplex red was selected as the indicator due to its enhanced sensitivity in glucose detection.[51] Fig. 5a illustrates this typical reaction for the colorimetric glucose assay. This enzymatic reaction can be
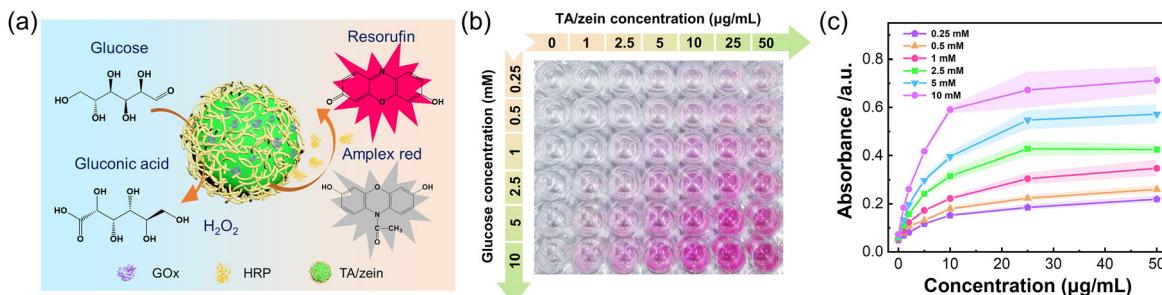
Fig. 5 (a) Schematic representation of enzymatic reactions using Amplex red. (b) Photographs depicting the colour change for different concentrations of TA/zein microparticles on varying glucose concentrations for 30 min. The red colour indicates the progression of the cascade reactions. (c) Changes in the absorbance of resorufin monitored at 570 nm.

divided into two steps: first, GOx catalyzes the conversion of glucose and O_2 into gluconic acid and H_2O_2. Then horseradish peroxidase (HRP) in the solution consumes the generated H_2O_2 to convert Amplex red to resorufin, resulting in a distinct red colour with peak absorbance at 570 nm. Therefore, this cascade enzymatic catalysis could induce a visible colour change in the reactant solution. We found that higher concentrations of

glucose and GOx@TA/zein microparticles resulted in a darker colour after the reaction (Fig. 5b). For precise detection and quantification, a microplate reader was employed to measure the absorbance at 570 nm of resorufin produced *via* the enzymatic reaction. Notably, changes in absorbance indicate that the resorufin concentration increased with the higher glucose and microparticle concentrations within the catalytic
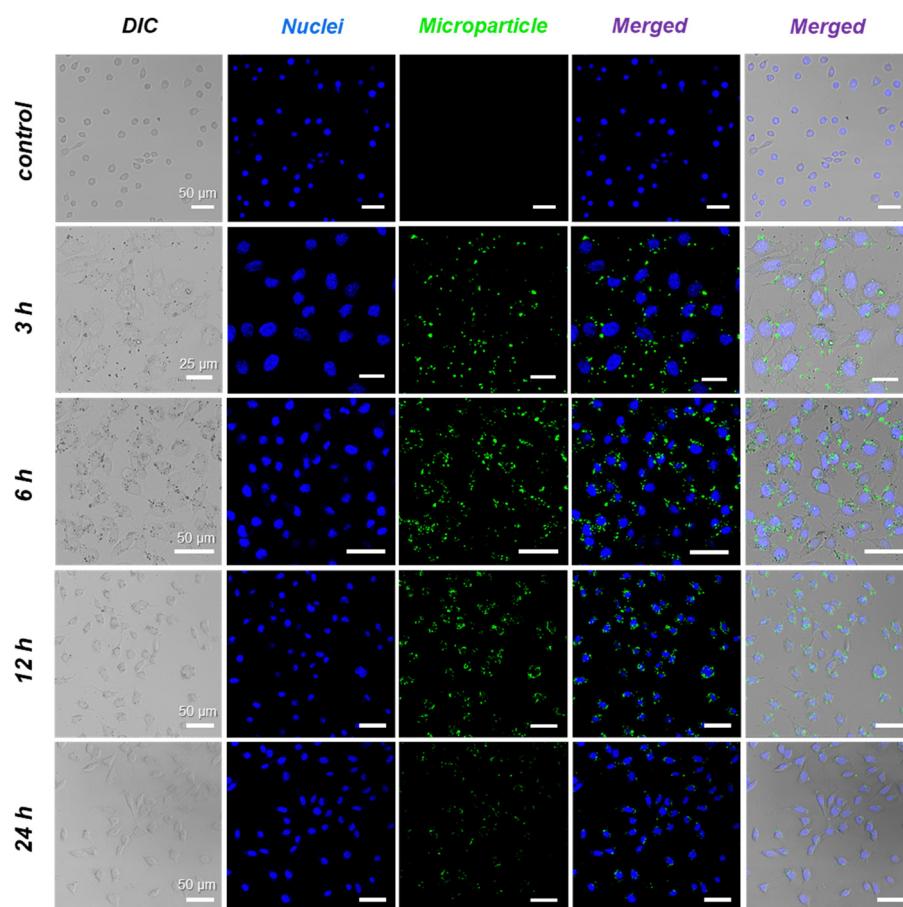

Fig. 6 Cellular uptake of TA/zein microparticles: CLSM images of intracellular uptake of FITC-dextran-loaded microparticles by HeLa cells. Cells were counter-stained with DAPI (for nuclei).
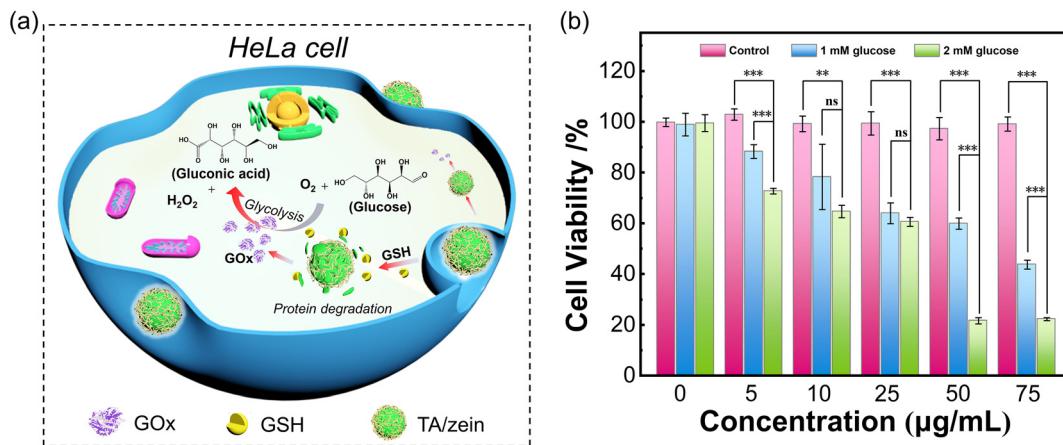
Fig. 7 (a) Schematic representation of the TA/zein microparticles entering the cell and releasing GOx. (b) *In vitro* cytotoxicity of the GOx-loaded microparticles. The effect of glucose concentration on cell viability under different concentrations of GOx@TA/zein microparticles. *$p < 0.05$, **$p < 0.01$, ***$p < 0.001$.

reaction for 30 min (Fig. 4c). Therefore, this result further proved that the activity of GOx can be well retained in TA/zein microparticles.

Cellular uptake of TA/zein microparticles

To further verify our hypothesis, HeLa cells were selected as representative tumor cells for investigating the phagocytosis and endocytosis of TA/zein microparticles, and the temporal change of particle distribution was recorded by CLSM. The cells were incubated with 10 μg mL^{-1} of TA/zein microparticles encapsulating FITC-dextran, while the nuclei of the cells were labelled with DAPI. Fig. 6 displays the uptake of TA/zein microparticles by HeLa cells at different incubation times. As shown in Fig. 6, no green fluorescence can be observed if there are no microparticles in the medium. When the incubation time was extended to 3 h, the presence of green fluorescent spots inside the cells became apparent. However, the number of endocytosed particles was limited and free particles were still observable. After 6 h of incubation, the green fluorescent spots around the nucleus (blue) became more pronounced, and the free microparticles became almost negligible, suggesting that the phagocytosis process is time-dependent. At this time point, we conducted a more detailed examination of the distribution of microparticles under higher magnification. To highlight the cell membrane, we stained it with actin-tracker red-rhodamine. It is evident that the green fluorescent spots were primarily dispersed in the cytoplasmic area while the nuclear region displayed no fluorescent signal, indicated by the arrows in Fig. S14 (ESI†). This observation proves that endocytosed microparticles did not enter the nucleus. When the incubation period was prolonged to 12 h, a decrease of the microparticles and fluorescence intensity inside the cells was observed. After 24 h of incubation, the green fluorescence inside the cells became much weaker. This phenomenon could be attributed to breaking of the disulfide bond by GSH, resulting in the rupture of the microparticles and release of encapsulated

FITC-dextran. As a result, the dye molecules diffused inside the entire cells and led to weaker fluorescence.

In vitro cytotoxicity of GOx@TA/zein microparticles

The MTT assay was utilized to evaluate the anticancer activity of the GOx-loaded microparticles. The effectiveness of the GOx-based starvation therapy mainly relies on glucose consumption and the production of a substantial quantity of H$_2$O$_2$, triggering cell apoptosis (Fig. 6a). Compared to traditional starvation therapy that only cuts off the glucose supply, the presence of GOx exhibits a stronger anticancer performance. Fig. 7b shows the effect of GOx@TA/zein microparticle concentration and glucose concentration on cytotoxicity. After 24 h of incubation, the control group displayed minimal cytotoxicity towards HeLa cells, with cell survival rates of approximately 100%. This result indicates that the transport carrier TA/zein microparticles are biocompatible materials with low cytotoxicity. On the contrary, the presence of GOx@TA/zein microparticles leads to a significant decline in cell viability particularly at a higher glucose concentration. For 50 μg mL^{-1} microparticle concentration, the addition of 1 mM glucose resulted in a 37% decrease in cell viability compared to the control group. When the glucose concentration was increased to 2 mM, cell viability significantly decreased to approximately 20%. This is mainly due to the rise in H$_2$O$_2$ levels with the increase in glucose, which exhibits strong biological toxicity and further induces apoptosis. A similar decreasing trend is also observed with an increase in the concentration of GOx@TA/zein microparticles, further confirming the therapeutic impact of these GOx-loaded microparticles.

3. Conclusions

In summary, this work presents a straightforward strategy to design and prepare biocompatible proteinaceous microparticles using the Pickering emulsion template. The adjustable

emulsification parameter allows us to prepare proteinaceous microparticles with tailored sizes and structures. Additionally, the introduction of TA can improve the dispersion of the microparticles in the aqueous medium. Furthermore, due to the presence of intramolecular and intermolecular disulfide bonds between zein proteins, the zein-based microparticles exhibited good GSH-responsiveness and could be decomposed in tumor cells with high GSH levels. Meanwhile, GOx was selected as a therapeutic biomolecule model and successfully encapsulated in microparticles for starvation therapy. The results demonstrated that the proposed method is bio-friendly, as the proteinaceous microparticles displayed low cytotoxicity and the encapsulated enzymes retained good catalytic activity. These findings suggest that the proteinaceous microparticles may serve as efficient, biocompatible, and biodegradable carriers for bio-molecules and hold promising prospects for future biomedical applications.

Author contributions

W. Jiang: data curation, investigation, and writing – original draft; X. Guan: investigation, resources, and writing – original draft; W. Liu and Y. Li: investigation and conceptualization; H. Jiang: conceptualization, supervision, writing – review & editing, and funding acquisition; T. Ngai: project administration, writing – review & editing, and supervision.

Conflicts of interest

The authors declare no conflict of interest.

Acknowledgements

References

1 B. S. Chhikara and K. Parang, *Chem. Biol. Lett.*, 2023, **10**, 1.

2 S. G. Liu, A. R. Khan, X. Y. Yang, B. Dong, J. B. Ji and G. X. Zhai, *J. Controlled Release*, 2021, **335**, 1–20.

3 B. J. Ma, S. Wang, F. Liu, S. Zhang, J. Z. Duan, Z. Li, Y. Kong, Y. H. Sang, H. Liu, W. B. Bu and L. L. Li, *J. Am. Chem. Soc.*, 2019, **141**, 849–857.

4 C. Xu and K. Y. Pu, *Chem. Soc. Rev.*, 2021, **50**, 1111–1137.

5 D. W. Zheng, B. Li, C. X. Li, J. X. Fan, Q. Lei, C. Li, Z. S. Xu and X. Z. Zhang, *ACS Nano*, 2016, **10**, 8715–8722.

6 C. Hennequin, S. Guillerm, S. Wong and L. Quéro, *Cancer Radiother.*, 2018, **22**, 367–371.

7 L. M. Riedmayr, K. S. Hinrichsmeyer, N. Karguth, S. Böhm, V. Splith, S. Michalakis and E. Becirovic, *Nat. Protoc.*, 2022, **17**, 781–818.

8 Y. H. Hu, H. J. Cheng, X. Z. Zhao, J. J. Wu, F. Muhammad, S. C. Lin, J. He, L. Q. Zhou, C. P. Zhang, Y. Deng, P. Wang, Z. Y. Zhou, S. M. Nie and H. Wei, *ACS Nano*, 2017, **11**, 5558–5566.

9 L. H. Fu, C. Qi, J. Lin and P. Huang, *Chem. Soc. Rev.*, 2018, **47**, 6454–6472.

10 O. Benyoseph and B. D. Ross, *Br. J. Cancer*, 1994, **70**, 1131–1135.

11 Q. Liu, A. M. Rauth, J. Liu, K. Babakhanian, X. Y. Wang, R. Bendayan and X. Y. Wu, *Pharm. Res.*, 2009, **26**, 2343–2357.

12 W. G. Zhao, J. Hu and W. P. Gao, *ACS Appl. Mater.*, 2017, **9**, 23528–23535.

13 R. J. Liang, Y. Chen, M. F. Huo, J. Zhang and Y. S. Li, *Nanoscale Horiz.*, 2019, **4**, 890–901.

14 Y. Zhang, Y. Yang, S. Jiang, F. Li, J. Lin, T. Wang and P. Huang, *Mater. Horiz.*, 2019, **6**, 169–175.

15 N. A. Kotov, *Science*, 2010, **330**, 188–189.

16 G. J. Weiss, J. R. Infante, E. G. Chiorean, M. J. Borad, J. C. Bendell, J. R. Molina, R. Tibes, R. K. Ramanathan, K. Lewandowski, S. F. Jones, M. E. Lacouture, V. K. Langmuir, H. Lee, S. Kroll and H. A. Burris, *Clin. Cancer Res.*, 2011, **17**, 2997–3004.

17 Y. Luo, P. Yan, X. Y. Li, J. W. Hou, Y. Wang and S. B. Zhou, *Biomacromolecules*, 2021, **22**, 4384–4394.

18 J. Y. Z. Wu, Y. F. Zhang, K. J. Jiang, X. Y. Wang, N. T. Blum, J. Zhang, S. S. Jiang, J. Lin and P. Huang, *Adv. Mater.*, 2022, **34**, 2200062.

19 N. N. Zhang, G. F. Shu, L. Shen, J. Y. Ding, E. Q. Qiao, S. J. Fang, J. J. Song, Y. Yang, Z. W. Zhao, C. Y. Lu, J. F. Tu, M. Xu, Y. Z. Du, M. J. Chen and J. S. Ji, *Nano Res.*, 2022, **15**, 5262–5272.

20 J. Q. Mu, Y. Y. Du, X. W. Li, R. Yan, H. P. Zhong, M. Y. Cai, N. Yu, J. C. Zhang, X. Y. Yuan, X. Hua and S. T. Guo, *Chem. Eng. J.*, 2022, **451**, 138554.

21 M. Okamoto and B. John, *Prog. Polym. Sci.*, 2013, **38**, 1487–1503.

22 N. Reddy and Y. Q. Yang, *Trends Biotechnol.*, 2011, **29**, 490–498.

23 W. L. Stoppel, C. E. Ghezzi, S. L. McNamara, L. D. Black and D. L. Kaplan, *Ann. Biomed. Eng.*, 2015, **43**, 657–680.

24 Y. K. Jo and D. Lee, *Small*, 2020, **16**, e1903736.

25 A. R. Patel and K. P. Velikov, *Curr. Opin. Colloid Interface*, 2014, **19**, 450–458.

26 Y. Luo and Q. Wang, *J. Appl. Polym. Sci.*, 2014, **131**, 40696.

27 Y. Zhang, L. Cui, F. Li, N. Shi, C. Li, X. Yu, Y. Chen and W. Kong, *Int. J. Pharm.*, 2016, **513**, 191–210.

28 F. Y. Dong, X. L. Dong, L. P. Zhou, H. H. Xiao, P. Y. Ho, M. S. Wong and Y. Wang, *Colloid. Surf., B*, 2016, **140**, 324–331.

29 Q. L. Chen, M. Wu, J. R. Yao, Z. Z. Shao and X. Chen, *J. Mater. Chem. B*, 2023, **11**, 4529–4538.

30 S. Kim and J. Xu, *J. Cereal Sci.*, 2008, **47**, 1–5.

31 P. H. Hsu and A. Almutairi, *J. Mater. Chem. B*, 2021, **9**, 2179–2188.

32 A. Bansal and M. C. Simon, *J. Cell Biol.*, 2018, **217**, 2291–2298.

33 F. Q. Schafer and G. R. Buettner, *Free Radical Biol. Med.*, 2001, **30**, 1191–1212.

34 J. Wang, Q. Pei, R. Xia, S. Liu, X. Hu, Z. Xie and X. Jing, *Chem. Mater.*, 2020, **32**, 10719–10727.

35 M. M. He, J. Li, H. S. Han, C. A. Borges, G. Neiman, J. J. Roise, P. Hadaczek, R. Mendonsa, V. R. Holm, R. C. Wilson, K. Bankiewicz, Y. M. Zhang, C. M. Sadlowski, K. Healy, L. W. Riley and N. Murthy, *Chem. Sci.*, 2020, **11**, 8973–8980.

36 B. J. Sun, C. Luo, X. B. Zhang, M. R. Guo, M. C. Sun, H. Yu, Q. Chen, W. Q. Yang, M. L. Wang, S. Y. Zuo, P. Y. Chen, Q. M. Kan, H. T. Zhang, Y. J. Wang, Z. G. He and J. Sun, *Nat. Commun.*, 2019, **10**, 3211.

37 Q. Zhong and M. Jin, *Food Hydrocolloids*, 2009, **23**, 2380–2387.

38 T. Suzuki, E. Sato, Y. Matsuda, H. Tada, K. Unno and T. Kato, *Chem. Pharm. Bull.*, 1989, **37**, 1051–1054.

39 L. Chen and M. Subirade, *Biomacromolecules*, 2009, **10**, 3327–3334.

40 L. N. Britton, *J. Surfactants Deterg.*, 1998, **1**, 109–117.

41 H. Jiang, X. Hu, Y. Li, C. Yang and T. Ngai, *Chem. Sci.*, 2021, **12**, 12463–12467.

42 H. Jiang, X. F. Hu, W. J. Jiang, X. Guan, Y. X. Li and T. Ngai, *Langmuir*, 2022, **38**, 12273–12280.

43 L. D. Liu, J. J. Wei, K. M. Ho, K. Y. Chiu and T. Ngai, *J. Colloid Interface. Sci.*, 2023, **629**, 559–568.

44 H. Jiang, Y. F. Sheng and T. Ngai, *Curr. Opin. Colloid Interface*, 2020, **49**, 1–15.

45 H. Jiang, L. Z. Hong, Y. X. Li and T. Ngai, *Angew. Chem., Int. Ed.*, 2018, **57**, 11662–11666.

46 J. W. J. de Folter, M. W. M. van Ruijven and K. P. Velikov, *Soft Matter*, 2012, **8**, 6807–6815.

47 P. Shi, J. Qin, X. Wu, L. Wang, T. Zhang, D. Yang, X. Zan and D. Appelhans, *ACS Appl. Mater.*, 2019, **11**, 39209–39218.

48 A. Scalbert, *Phytochemistry*, 1991, **30**, 3875–3883.

49 N. C. Denko, *Nat. Rev. Cancer*, 2008, **8**, 705–713.

50 M. G. V. Heiden, L. C. Cantley and C. B. Thompson, *Science*, 2009, **324**, 1029–1033.

51 S. M. Jo, J. Kim, J. E. Lee, F. R. Wurm, K. Landfester and S. Wooh, *Adv. Sci.*, 2022, **9**, 2204665.